QUALITY AND EFFECTIVENESS OF GEOMETRIC APPROACH SOLVING WATER SURFACE AND UNDERWATER OBJECT POINTS

Kuan-Chen Lee[1], Jen-Jer Jaw[1]
[1]Dept. of Civil Engineering, National Taiwan University, Taiwan,
Email: r05521120@ntu.edu.tw, jejaw@ntu.edu.tw

KEY WORDS: Refraction, Water surface, Underwater object points, Influential factors

ABSTRACT: To deal with photogrammetric intersection considering the refraction effect in the functional model, where the camera and the object of interest are not as usual in the same optical media, only by quality object-to-image correspondence could lead to the whole path of imaging ray being correctly established. That is, the multi-media geometry has to be incorporated into geometric models. Therefore, the extension of standard photogrammetric imaging models adding Snell's Law for handling refraction effects is absolutely required. Under the assumption of all involved media being both homogeneous and isotropic, this study adopts piercing points to play a role of supporting points of the image ray through the interfaces of the different media. Besides, this study also aims to determine the underwater object points and the water surface simultaneously in air-to-water photogrammetry. Subsequently, the pseudo-observations are drawn into the adjustment model to offer great flexibility in adopting priori information of parameters so that the uncertainties of orientation parameters, refractive index, and image point measurement can be individually or unitedly considered. This study is concluded by reporting the quality and the effectiveness of the proposed approach in determining underwater object points and water surface.

1. INTRODUCTION

To achieve correct photogrammetric measurement results in multi-media environments, where the camera and the object of interest are not in the same optical media as before, the multi-media geometry must be incorporated into geometric models. Therefore, the extension of standard photogrammetric imaging models which can be used by Snell's Law for the handling of refraction effects occurring between varied optical media is absolutely required. The proposed module describes the solvability analysis both on the positions of underwater object points and the interface planarity, where the object in water is observed by cameras in air through one water surface. The study presents a unified approach to research on qualitative and quantitative discussion of accuracy potential, which can be implement as a reference for future similar scenes and measurement tasks.

With the ever-changing photogrammetry technology, a wide range of application scenarios like multi-media environments have gradually gained increased importance over the last decades (Maas, 2015). Generally, the collinearity condition in basic assumption connects image coordinates, camera projection center and object point coordinates forming a straight line, but sometimes need to deal with optical rays at the transition between optical media with different refractive indices. The optical ray between the perspective center of the camera and an object point changes from a straight line to a poly-line, with the object point as start and the corresponding image point as the end. To reconstruct the actual ray path, assume that all the passed media are homogeneous and isotropic. The piercing points play a role of the supporting points of the image ray through the interfaces of the different media. Subsequently, several extensions of the model will be introduced. The other part of the project addresses some influential factors which may affect the accuracy potential of underwater photogrammetry, such as exterior and interior orientation parameters, image point coordinates, refractive index, and underwater object point coordinates.

In the following, many papers were published in the past dealing with the stereo-pair photogrammetry principle, where the two conjugate rays from both left and right intersect at the same point to compute the coordinates of targets. However, the simultaneously determination of the underwater object points and the water surface is limited to intersection geometry (Chiu and Jaw, 2016), or so-called the angle of intersection, and insufficient redundancy under the situation. Even the water surface changes and other issues. For this reason, the proposed approach includes joint solution analysis of single image pairs of multiple sets of conjugate points to improve the number of observations on the water surface. Also, concentrating on how to improve geometric model and further reduce the degradation of the quality of results by not only the qualitative discussions of solvability and the strategies solving for singular geometry, but also the quantitative analysis of the quality of determined underwater object points and the water surface. Using the standard deviations and covariance of variables to discuss the correlation amounts to significant findings as the effects of intersection while determining the water surface. The last part of the study especially dealing with intersecting performance of conjugate ray with unknown water surface and taking the factors of uncertainty of orientation parameters, image point measurements and refractive index of water into main consideration. Meanwhile, the results of stereo-pair intersection adopting single point or two points are compared later.

2. MATERIALS AND METHODS

Many approaches of multi-media photogrammetry require the 3D coordinates of objects directly used as the observation in the geometric model. As an image ray passing through media with different refractive index, the traditional collinearity of the image point, the projection center and the object point is no longer the same as before. Therefore, the object point coordinates must be corrected by a multi-media module in order to reconstruct the actual optical path and meet the collinearity equations again. In the proposed mathematical model, the main idea combines with many approaches, like (Maas and Gruen, 1995) or (Kotowski, 1987), who once introduced a multi-media module into the collinearity equations. And based on (Huang and Jaw, 2014), who developed a ray-tracing method by Snell's Law, to interpret the refraction effects taking place on the water surface containing the interface normal vector and the ray incident vector. In this paper, according to the imaging path, the object-to-image correspondence is divided into two parts, namely the air vector and the water vector (see Figure 1). The mathematical relationship in detail is described later.

2.1 The Air-to-Water Photogrammetry Intersection

Collinearity, a valid principle for one medium, yet does not prevail in multimedia. To maintain conventional collinear characteristic, the air-water photogrammetry model offers an adaptation to the two-media environment. The imaging system is described by the following parameters: $\boldsymbol{A} = (X_A, Y_A, Z_A)$, the 3D coordinates of the known objects in the simulated data; $\boldsymbol{L} = (X_L, Y_L, Z_L)$, the perspective center (camera position); $\boldsymbol{R_i}(i = 1\sim3)$, the row vectors of the camera rotation matrix $\boldsymbol{R}$; $\boldsymbol{P} = (X_P, Y_P, Z_P)$, the piercing point coordinates of the image ray, which can be directly computed; (x_a, y_a), the image coordinates of known object points; (x_0, y_0), the image coordinates of principal point; f, the principal distance; and $\langle \cdot, \cdot \rangle$, the inner product.

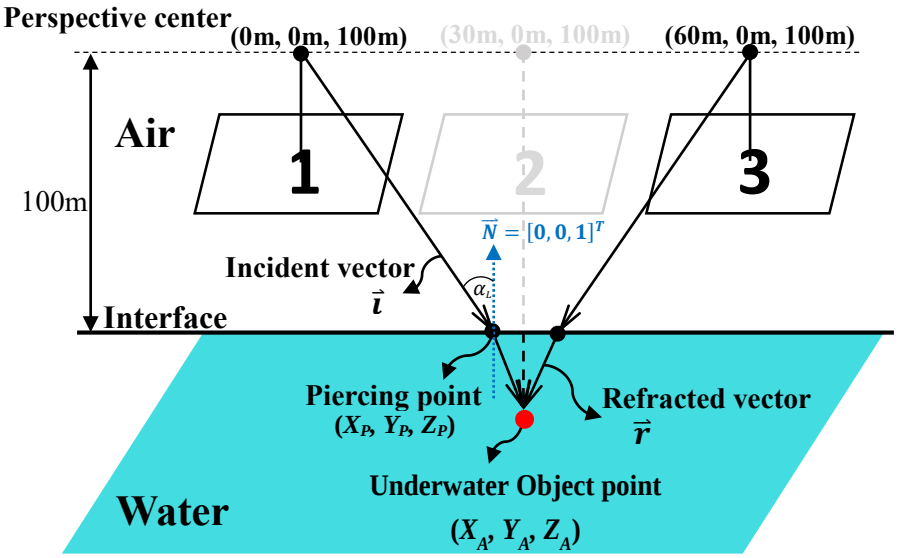

Figure 1. The air-to-water geometric model.

In the air vector part, we begin with the standard collinearity equations as follows:

$$\begin{cases} x_a = x_0 - f\dfrac{\langle \boldsymbol{R_1}, \boldsymbol{P}\rangle - \langle \boldsymbol{R_1}, \boldsymbol{L}\rangle}{\langle \boldsymbol{R_3}, \boldsymbol{P}\rangle - \langle \boldsymbol{R_3}, \boldsymbol{L}\rangle} \\ y_a = y_0 - f\dfrac{\langle \boldsymbol{R_2}, \boldsymbol{P}\rangle - \langle \boldsymbol{R_2}, \boldsymbol{L}\rangle}{\langle \boldsymbol{R_3}, \boldsymbol{P}\rangle - \langle \boldsymbol{R_3}, \boldsymbol{L}\rangle} \end{cases} \tag{1}$$

If the optical ray passes through the interface $Z = 0$, then the normal vector is defined as $\vec{\boldsymbol{N}} = [0,0,1]^T$. The incoming light ray $\vec{\boldsymbol{i}} = [X_P - X_L, Y_P - Y_L, Z_P - Z_L]^T$, is formed from the perspective point to the piercing point. The angles of incidence can be introduced as functions of the normal vector as well as the incident vector:

$$\alpha = \cos^{-1}\left(\frac{\langle \vec{i}, \vec{N}\rangle}{|\vec{i}||\vec{N}|}\right) \tag{2}$$

And the angles of refraction can be derived by using Snell's Law, which is described as follows (with n_a and n_w the refractive indices of air and water, respectively):

$$\beta = \sin^{-1}\left(\sin(\alpha) * \frac{n_a}{n_w}\right) \tag{3}$$

The normalized rotation axis $\bar{\boldsymbol{\tau}} = [\mathrm{a}, \mathrm{b}, \mathrm{c}]^T$ generated by the product of the entering vector and the normal vector, as well as the rotation angles θ derived from the difference between α, the angle of incidence, and β, the angle of refraction, will be used to form the rotation matrix $\boldsymbol{M}$, which rotates the incident vector and thus constitutes the normalized refracted vector,

$$\vec{\boldsymbol{r}} = \langle \boldsymbol{M}, \vec{\boldsymbol{\imath}}/|\vec{\boldsymbol{\imath}}| \rangle \tag{4}$$

with

$$\boldsymbol{M} = \begin{bmatrix} \mathrm{a}^2(1-\cos\theta)+\cos\theta & \mathrm{ab}(1-\cos\theta)-\mathrm{c}\sin\theta & \mathrm{ac}(1-\cos\theta)+\mathrm{b}\sin\theta \\ \mathrm{ab}(1-\cos\theta)+\mathrm{c}\sin\theta & \mathrm{b}^2(1-\cos\theta)+\cos\theta & \mathrm{bc}(1-\cos\theta)-\mathrm{a}\sin\theta \\ \mathrm{ac}(1-\cos\theta)-\mathrm{b}\sin\theta & \mathrm{bc}(1-\cos\theta)+\mathrm{a}\sin\theta & \mathrm{c}^2(1-\cos\theta)+\cos\theta \end{bmatrix} \tag{5}$$

Finally, according to redefining the object-to-image correspondence, the ray path can be obtained from the vector relationship between air and water. To define the modified collinearity equations, we make use of a virtual imaging system consisting of the water surface as the modified image plane. The image coordinates in the new system can be written as

$$\begin{cases} F_x = X_P + \boldsymbol{r_x} * \left(\frac{Z_A - d}{\boldsymbol{r_z}}\right) - X_A \\ F_y = Y_P + \boldsymbol{r_y} * \left(\frac{Z_A - d}{\boldsymbol{r_z}}\right) - Y_A \end{cases} \tag{6}$$

The air-to-water imaging geometry has been set up by the relationship between vectors of incoming and leaving light rays. The equation system consists of two equations with unknown coordinates and unknown water surface for single ray and only one object point in photogrammetry intersection. Due to the quadratic structure of the system and the nonlinear character, Newton's iterative method has to be used for solving.

2.2 Least-Squares Adjustment with Unified Approach

Traditionally, some variables involved in a least-squares (LS) adjustment can be treated as observations and parameters, respectively. However, the unified approach is an alternative method where some of the variables in the mathematical model are treated as observations by means of assigning a priori weights to them (Mikhail, 1976). In the following, both the general model to least-squares and the unified approach to least-squares are drawn into the random model that leads the adjustment more reasonable and flexible. Since the observations and parameters in above equations are implicitly related, the linearized adjustment model, or so-called Guass-Helmert model (Mikhail, 1976) is used as Eq. (7). The linearized condition equations are as below:

$$\begin{gathered} \underset{r\times m}{\boldsymbol{B}}\underset{m\times 1}{\boldsymbol{V}} + \underset{r\times u}{\boldsymbol{A}}\underset{u\times 1}{\boldsymbol{X}} + \underset{r\times u'}{\bar{\boldsymbol{A}}}\underset{u'\times 1}{\bar{\boldsymbol{X}}} = \underset{r\times 1}{\boldsymbol{W}}, \qquad \boldsymbol{V} \sim (0, \Sigma = {\sigma_0}^2 \boldsymbol{Q} = {\sigma_0}^2 \boldsymbol{P}^{-1}) \\ (r = 2np;\ \ m = 2np;\ \ u = 3p{+}1;\ \ u' = 1{+}3{+}6n) \end{gathered} \tag{7}$$

$$\boldsymbol{V}_{\bar{\boldsymbol{X}}} - \bar{\boldsymbol{X}} = {\boldsymbol{L}_{\bar{\boldsymbol{X}}}}^0 - {\boldsymbol{L}_{\bar{\boldsymbol{X}}}}^{\mathrm{obs}} = \boldsymbol{W}_{\bar{\boldsymbol{X}}}, \qquad \boldsymbol{V}_{\bar{\boldsymbol{X}}} \sim (0, \Sigma = {\sigma_0}^2 \boldsymbol{Q}_{\bar{\boldsymbol{X}}\bar{\boldsymbol{X}}} = {\sigma_0}^2 {\boldsymbol{P}_{\bar{\boldsymbol{X}}}}^{-1}) \tag{8}$$

where $\boldsymbol{A}$, $\bar{\boldsymbol{A}}$ and $\boldsymbol{B}$ are the matrices of derivatives with respect to the unknowns, influential factors and image observations, respectively, $\boldsymbol{W}$ and $\boldsymbol{W}_{\bar{\boldsymbol{X}}}$ denote misclosure vectors, ${\boldsymbol{L}_{\bar{\boldsymbol{X}}}}^0$ is the vector that stores the approximate values of the vector of factors $\bar{\boldsymbol{X}}$, ${\boldsymbol{L}_{\bar{\boldsymbol{X}}}}^{\mathrm{obs}}$ denotes "observed" values of the factors, and $\boldsymbol{V}_{\bar{\boldsymbol{X}}}$ is the vector of residuals associated with the "observed" parameters. It should be noted that $\boldsymbol{X}$ and $\bar{\boldsymbol{X}}$ denote corrections to the unknowns and the factors themselves if the latter can be estimated directly. The above equations can be combined into one, and written as:

$$\begin{bmatrix} \boldsymbol{B} & & & \\ & \underset{1\times 1}{\boldsymbol{I}} & & \\ & & \underset{3\times 3}{\boldsymbol{I}} & \\ & & & \underset{6n\times 6n}{\boldsymbol{I}} \end{bmatrix} \begin{bmatrix} \boldsymbol{V} \\ \boldsymbol{V}_{n_w} \\ \boldsymbol{V}_{IOP} \\ \boldsymbol{V}_{EOP} \end{bmatrix} + \begin{bmatrix} \boldsymbol{A} & \boldsymbol{A}_{n_w} & \boldsymbol{A}_{IOP} & \boldsymbol{A}_{EOP} \\ & \underset{1\times 1}{-\boldsymbol{I}} & & \\ & & \underset{3\times 3}{-\boldsymbol{I}} & \\ & & & \underset{6n\times 6n}{-\boldsymbol{I}} \end{bmatrix} \begin{bmatrix} \boldsymbol{X} \\ \boldsymbol{X}_{n_w} \\ \boldsymbol{X}_{IOP} \\ \boldsymbol{X}_{EOP} \end{bmatrix} = \begin{bmatrix} \boldsymbol{W} \\ \boldsymbol{W}_{n_w} \\ \boldsymbol{W}_{IOP} \\ \boldsymbol{W}_{EOP} \end{bmatrix} \tag{9}$$

where the matrix $\boldsymbol{A}$ and each of the vectors $\bar{\boldsymbol{X}}$, $\boldsymbol{W}_{\bar{\boldsymbol{X}}}$ and $\boldsymbol{V}_{\bar{\boldsymbol{X}}}$ have been decomposed, for the sake of convenience, into three four parts corresponding to object point coordinates ($\boldsymbol{A}$, $\boldsymbol{X}$, $\boldsymbol{W}$, $\boldsymbol{V}$), $\mathrm{n_w}$ ($\boldsymbol{A}_{n_w}$, $\boldsymbol{X}_{n_w}$, $\boldsymbol{W}_{n_w}$, $\boldsymbol{V}_{n_w}$), IOPs ($\boldsymbol{A}_{IOP}$, $\boldsymbol{X}_{IOP}$, $\boldsymbol{W}_{IOP}$, $\boldsymbol{V}_{IOP}$) and EOPs ($\boldsymbol{A}_{EOP}$, $\boldsymbol{X}_{EOP}$, $\boldsymbol{W}_{EOP}$, $\boldsymbol{V}_{EOP}$). The system of normal equations for $\hat{\boldsymbol{X}}$ can be written as follows:

$$\boldsymbol{N}\hat{\boldsymbol{X}} = \boldsymbol{U} \tag{10}$$

with

$$\boldsymbol{N} = \begin{bmatrix} \boldsymbol{A}^T\boldsymbol{M_e}\boldsymbol{A} & \boldsymbol{A}^T\boldsymbol{M_e}\boldsymbol{A}_{n_w} & \boldsymbol{A}^T\boldsymbol{M_e}\boldsymbol{A}_{IOP} & \boldsymbol{A}^T\boldsymbol{M_e}\boldsymbol{A}_{EOP} \\ \boldsymbol{A}_{n_w}^T\boldsymbol{M_e}\boldsymbol{A} & \boldsymbol{A}_{n_w}^T\boldsymbol{M_e}\boldsymbol{A}_{n_w} + \boldsymbol{P}_{n_w} & \boldsymbol{A}_{n_w}^T\boldsymbol{M_e}\boldsymbol{A}_{IOP} & \boldsymbol{A}_{n_w}^T\boldsymbol{M_e}\boldsymbol{A}_{EOP} \\ \boldsymbol{A}_{IOP}^T\boldsymbol{M_e}\boldsymbol{A} & \boldsymbol{A}_{IOP}^T\boldsymbol{M_e}\boldsymbol{A}_{n_w} & \boldsymbol{A}_{IOP}^T\boldsymbol{M_e}\boldsymbol{A}_{IOP} + \boldsymbol{P}_{IOP} & \boldsymbol{A}_{IOP}^T\boldsymbol{M_e}\boldsymbol{A}_{EOP} \\ \boldsymbol{A}_{EOP}^T\boldsymbol{M_e}\boldsymbol{A} & \boldsymbol{A}_{EOP}^T\boldsymbol{M_e}\boldsymbol{A}_{n_w} & \boldsymbol{A}_{EOP}^T\boldsymbol{M_e}\boldsymbol{A}_{IOP} & \boldsymbol{A}_{EOP}^T\boldsymbol{M_e}\boldsymbol{A}_{EOP} + \boldsymbol{P}_{EOP} \end{bmatrix} \tag{11}$$

and

$$\boldsymbol{U} = \begin{bmatrix} \boldsymbol{A}^T\boldsymbol{M_e}\boldsymbol{W} \\ \boldsymbol{A}_{n_w}^T\boldsymbol{M_e}\boldsymbol{W} - \boldsymbol{P}_{n_w}\boldsymbol{W}_{n_w} \\ \boldsymbol{A}_{IOP}^T\boldsymbol{M_e}\boldsymbol{W} - \boldsymbol{P}_{IOP}\boldsymbol{W}_{IOP} \\ \boldsymbol{A}_{EOP}^T\boldsymbol{M_e}\boldsymbol{W} - \boldsymbol{P}_{EOP}\boldsymbol{W}_{EOP} \end{bmatrix} \tag{12}$$

where

$$\boldsymbol{M_e} = (\boldsymbol{BQB}^T)^{-1} \tag{13}$$

The solution becomes

$$\widehat{\boldsymbol{X}} = \boldsymbol{N}^{-1}\boldsymbol{U} \tag{14}$$

And the vectors of residuals concerned with the observations and "observed" parameters are calculated as

$$\boldsymbol{V} = \boldsymbol{Q_{ll}}\boldsymbol{QB}^T\boldsymbol{M_e}(\boldsymbol{W} - \boldsymbol{AX}) \tag{15}$$

and

$$\boldsymbol{V}_{\bar{\boldsymbol{X}}} = \boldsymbol{W}_{\bar{\boldsymbol{X}}} + \bar{\boldsymbol{X}} \tag{16}$$

When the parameter correction is less than the threshold or the convergence condition, it means that the iteration is stopped. At the beginning of the LS adjustment, it is assumed that the prior variance factor σ_0^2 (a unitless quantity) is equal to 1.0. As the number of observations is larger than the number of unknown parameters, the posterior standard deviation factor can be computed

$$\hat{\sigma}_0 = \pm\sqrt{\frac{\boldsymbol{V^TPV} + \boldsymbol{V}_{\bar{\boldsymbol{X}}}{}^T\boldsymbol{P}_{\bar{\boldsymbol{X}}}\boldsymbol{V}_{\bar{\boldsymbol{X}}}}{d.o.f.}} \tag{17}$$

Therefore, calculating the posteriori variance-covariance matrix of them, and extracting the root of the matrix corresponding diagonal (variance) element that can be used as the theory precision of parameters.

$$\boldsymbol{\Sigma}_{\hat{\boldsymbol{X}}\hat{\boldsymbol{X}}} = \hat{\sigma}_0{}^2\boldsymbol{N}^{-1} \tag{18}$$

2.3 Analysis on the Equation System

This study focuses on the simultaneous solution of the coordinates of the underwater object point and the height of the water surface. Due to the quadratic structure of the system and the nonlinear character, iterative computation method has to be used for reaching the convergent solution. In the case of adopting two perspective centers, then the equation system consists of four equations with three unknown coordinates ($\boldsymbol{X_A}, \boldsymbol{Y_A}, \boldsymbol{Z_A}$) for an underwater object point A and one water surface parameter ($\boldsymbol{d}$). That is, the redundancy for this condition is equal to 0 as in Table 1.

Table 1. The number of requirements for solving the air-to water intersection.

For *n* conjugated rays intersect on *m* object points and one water surface	
Num. of observations	2*n*m
Num. of unknowns	3*m+1
Redundancy	(2*n-3)*m-1
Minimum num. of object points	m≥1

(where m = the number of object points; n = the number of conjugated rays (n≥2))

2.4 The Indicator for Accuracy Assessment

To properly represent the quality of the calculated results, one indicator for accuracy assessment is theoretical precision, which is the posterior precision of unknown parameters by adjustment. Another is the empirical accuracy by root-mean-square error, which can be computed from the most probable value of the random error given repeatedly.

Table 2. The indicator for representing the quality of solutions.

Theoretical Precision	**Empirical Accuracy**
$\begin{cases} \sigma_0 = \pm 1 \\ \hat{\sigma}_0 = \pm\sqrt{\dfrac{V^T(BQ_{ll}B^T)^{-1}V + V_x{}^TQ_{xx}{}^{-1}V_x}{d.o.f.}} \end{cases}$ $\Sigma_{\Delta\Delta} = \hat{\sigma}_0{}^2(\bar{A}^T(\bar{B}\bar{Q}\bar{B}^T)^{-1}\bar{A})^{-1} = \hat{\sigma}_0{}^2\boldsymbol{N}^{-1}$	$RMSE_X = \sqrt{\dfrac{\sum_{i=1}^{n}(\bar{X}_i - X)^2}{n}}$ $X = the\ true\ value\ of\ unknowns$ $\bar{X}_i = the\ mean\ value\ of\ unknowns$ $(by\ repeating\ n\ times)$

3. THE AIR-TO-WATER SCENE SIMULATION

The scene includes the object point coordinates of X component from -15 to 75 meters per 1 meter, Y component from -30 to 30 meters at 10 meter intervals, and Z component using -1, -5 and -9 meters respectively to build a point. The simulation results are as follows:

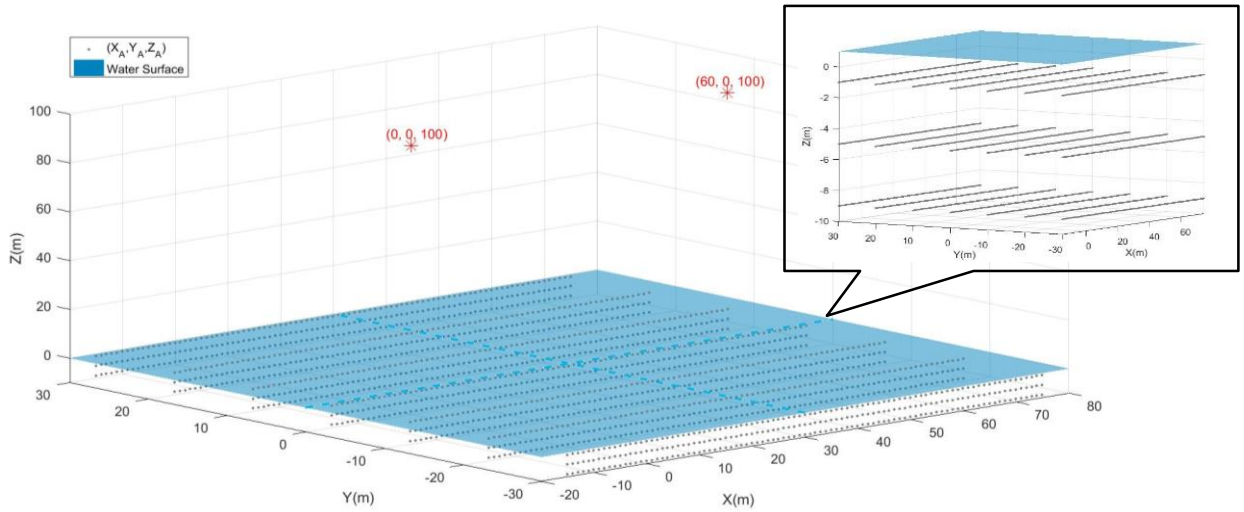

Figure 4. Simulation setup: the air-to-water photogrammetry scene.

For a rigorous validation of the proposed model, the simulated flight vehicle moves in the X-axis direction from (0m, 0m, 100m), with the base-height ratio (B/H) 0.6 as well as the ground sample distance (GSD) about 3 cm. To properly represent how the parameters applied in the simulated setting can affect the positioning precision, list all parameters and their corresponding values in Table 3.

Table 3. The simulated parameters in the air-to water intersection.

Parameter			**Value**		
Refractive index of air		n_a	1.00		
Refractive index of water		n_w	1.33		
Interior orientation [mm]		(x_0, y_0)	(0,0)		
		f	24		
pixel sixe [mm]			0.0064		
image size [mm]			36×24		
Base-Height ratio		B/H	≈ 0.6		
Ground sample distance [cm]		GSD	2.6 ~ 2.9		
			Photo 1	**Photo 2**	**Photo 3**
Exterior orientation	[m]	(X_L,Y_L,Z_L)	(0,0,100)	(30,0,100)	(60,0,100)
	[°]	(ω,φ,κ)	(0,0,0)	(0,0,0)	(0,0,0)

Note that the GSD, used to define the distance between pixel centers measured on the ground, will be changed with the elevation difference between perspective centers and underwater object points. For example, give a camera position of (0m, 0m, 100m) as in Photo 1 (see Table 3) and three unknown object point which is at Z = -1m, -5m and -9m respectively to clearly denote their ground sample distance for a corresponding orthophoto (Figure 5)

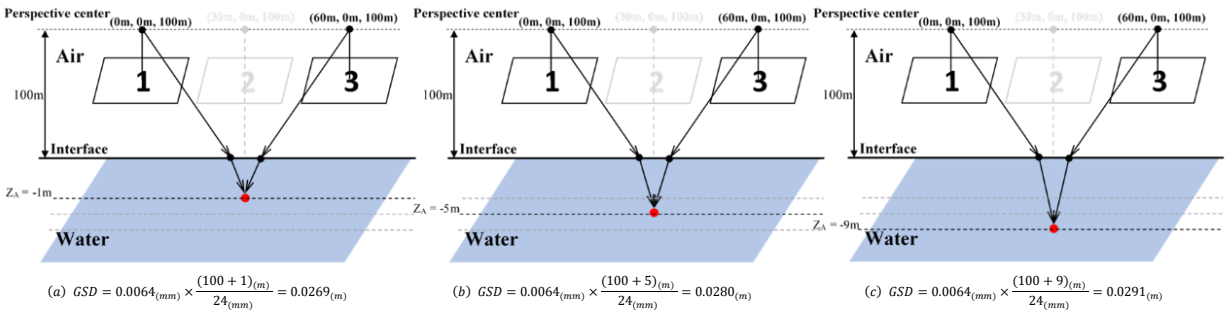

(a) $GSD = 0.0064_{(mm)} \times \frac{(100+1)_{(m)}}{24_{(mm)}} = 0.0269_{(m)}$ (b) $GSD = 0.0064_{(mm)} \times \frac{(100+5)_{(m)}}{24_{(mm)}} = 0.0280_{(m)}$ (c) $GSD = 0.0064_{(mm)} \times \frac{(100+9)_{(m)}}{24_{(mm)}} = 0.0291_{(m)}$

Figure 5. The Illustration of varied GSD values in simulated geometry.

4. ANALYSIS AND RESULTS

To clearly define the end results which are supposed to meet some prior information such as the ground sample distance (GSD), just insert the random error for observations of image point coordinates (σ_{xa}, σ_{ya}) into intersection adjustment. Based on the authors' preliminary study in backward projection, a process of tracing the image point given an object point, the offsets of imaging results shown before and after adding water into the scene will be at least 1 pixel. Therefore, assume the random error brought in the observations for 1-pixel size, that is, 0.0064mm. The computed strategies can be divided into three situations:
(1) air-to-water intersection for known water surface;
(2) air-to-water intersection for unknown water surface;
(3) air-to-water intersection for unknown water surface and joint multiple points.

4.1 The Solvability Analysis of Water Surface and Underwater Object Point Coordinates

As the condition number of a function is related to an argument measures or parameters of small errors for the sensitivity and stability of the whole solution system. That is, it can be used as a basic tool for how much the output value of the function can change due to a small change in the input argument. The larger the condition number, that a smaller error can lead to dramatic changes in the lack of geometric strength and easy to be rank-defected; otherwise, the solution system tends to be stable.

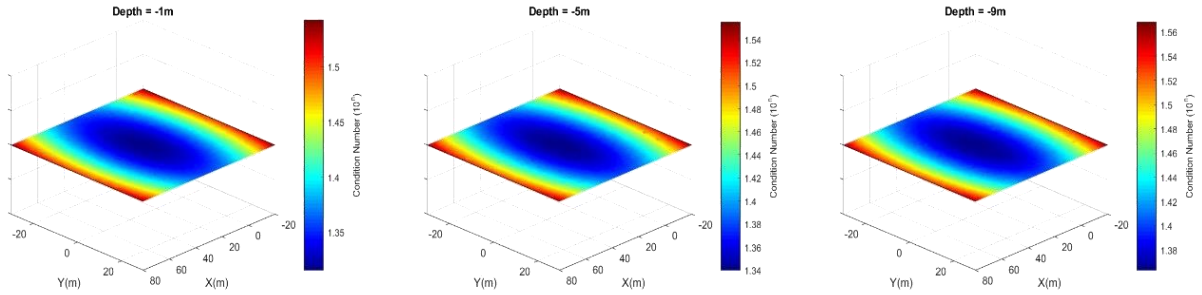

Figure 6. The value of condition number corresponding to different water depth (for known water surface).

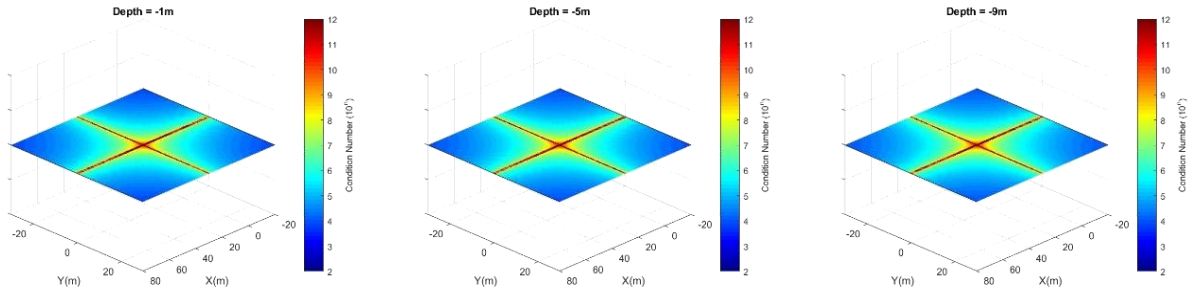

Figure 7. The value of condition number corresponding to different water depth (for unknown water surface).

Therefore, the condition number of the solution system would help to evaluate the geometric strength. Under the scenario of single point intersection, it is observed that the position and distribution of the singularity (also found rank deficiency) occurs for those points situated on the vertical plane passing through the baseline and those on the plane perpendicular to and passing through the middle of the baseline. On the other hand, when it comes to employing multiple points intersection, the variations of condition number when dealing with water surface and underwater object point coordinates are drawn in Figure 8 assuming that each point is considered with one corner point (Point 1, 5552 and 11103 with respect to the depth -1m, -5m and -9m), respectively.

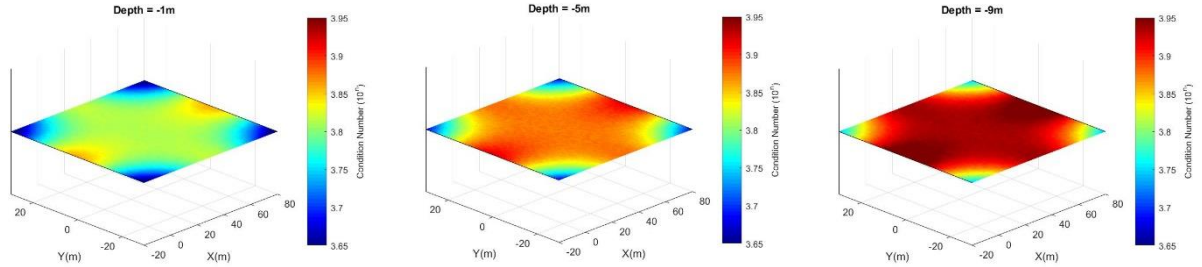

Figure 8. The condition number corresponding to two points with different water depth (for unknown water surface).

When using single point to solve the intersection, the minimum number of conditions can be satisfied. However, there is a problem that the quality of the results at varied positions is different from each other. Therefore, we can use joint solution to explore how to use the minimum points (e.g. 2) to improve the overall accuracy of the settlement and make the quality of water surface tend to stabilize and improve this phenomenon. By adding one corner point which has less condition number to solvability analysis of single point intersection, the following conclusions from the results of this section were performed:

- The condition number increases with the depth of the underwater points.
- In Figure 8, the results get significantly better than in Figure 7 and are only by approximately a factor 2 or 3 worse than in Figure 6. Some points are no longer prone to be rank-defected as before.
- For the points near the corner of the simulated scene, the condition number is still similar as before, and the solution system tends to be stable.

4.2 Correlation Analysis on Single Point/Two Points by Stereo-Pair Intersection

The correlation coefficient is a measure of the linear correlation between two variables, derived from their covariance divided by the product of their standard deviations. The following results in Figure 9 and Figure 10 are drawn by adopting single point and multiple points intersection respectively, representing the correlation between (d) and (X_A, Y_A, Z_A).

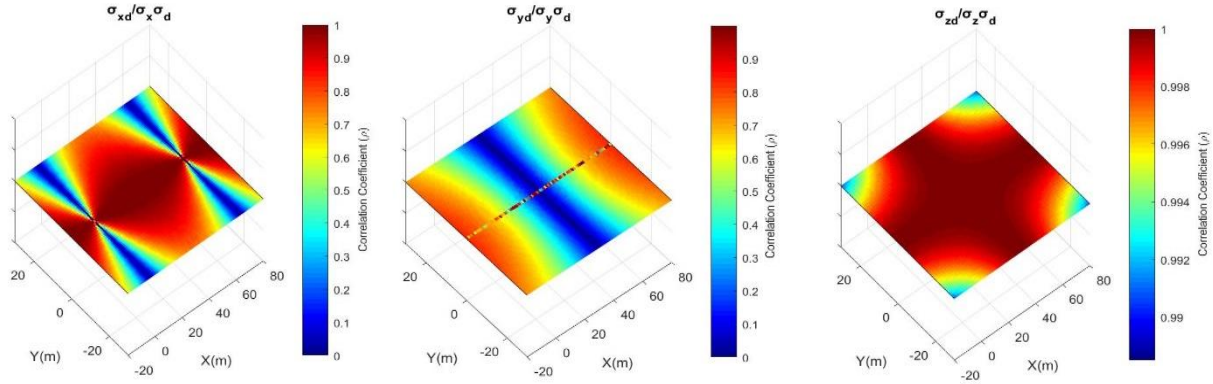

Figure 9. The correlation coefficient from single point intersection.

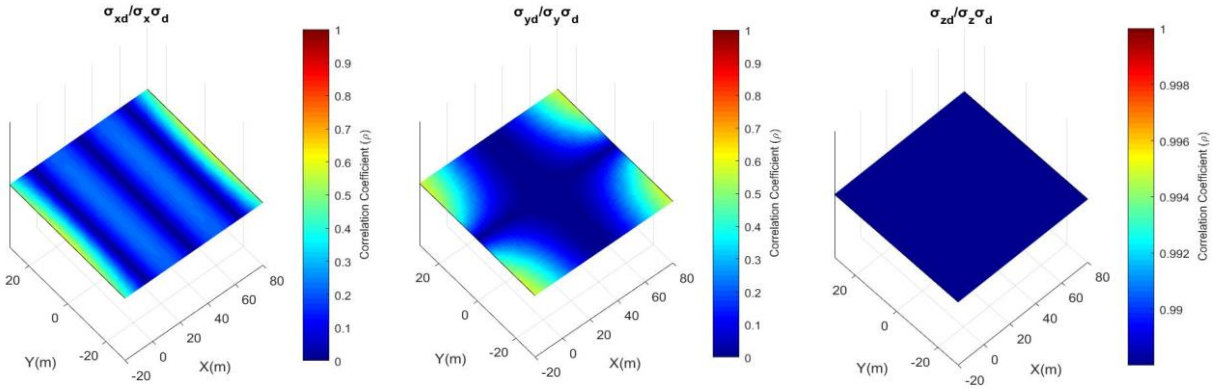

Figure 10. The correlation coefficient from two points intersection.

Considering that if there is a high correlation between variables, it is prone to have a strong relationship between each other. However, when regarding one corner point as another target point, the correlation between Z component and water surface has a further significant degradation than single point solution, so does X and Y component.

4.3 Impacts of Influential Factors

To analyze on how the uncertainty of each factor affects the positioning outcome, adopt an object point (Point 1) located at the corner of the simulated configuration as in Table 4.

Table 4. Influence of each factor on XYZ component and water surface (d) for Point 1 (-15, -30, -1).

Factors	**Random error**	**Quality of object point coordinates (m)**			**Quality of water surface (m)**
		±RMSE$_X$/ $\pm\tilde{\sigma}_X$	**±RMSE$_Y$/ $\pm\tilde{\sigma}_Y$**	**±RMSE$_Z$/ $\pm\tilde{\sigma}_Z$**	**±RMSE$_d$/ $\pm\tilde{\sigma}_d$**

Image coordinates	(x_a, y_a)	±0.0064mm	0.037/ 0.042	0.031/ 0.039	0.546/ 0.651	1.030/ 1.190
		±0.0128mm	0.087/ 0.083	0.070/ 0.078	1.179/ 1.298	2.112/ 2.374
		±0.0192mm	0.110/ 0.125	0.105/ 0.117	1.586/ 1.936	2.864/ 3.538
E.O.	X_L, Y_L	±0.01m	0.016/ 0.016	0.014/ 0.015	0.224/ 0.241	0.401/ 0.441
		±0.02m	0.026/ 0.031	0.025/ 0.029	0.387/ 0.483	0.720/ 0.882
		±0.05m	0.074/ 0.078	0.076/ 0.073	1.068/ 1.206	1.920/ 2.205
	Z_L	±0.03m	0.0000/ 0.000	0.0000/ 0.000	0.167/ 0.184	0.383/ 0.426
		±0.05m	0.0000/ 0.000	0.0000/ 0.000	0.232/ 0.307	0.532/ 0.710
		±0.10m	0.0000/ 0.000	0.0000/ 0.000	0.504/ 0.613	1.239/ 1.419
	ω	±0.0005°	0.001/ 0.001	0.001/ 0.001	0.023/ 0.023	0.042/ 0.042
		±0.005°	0.008/ 0.008	0.011/ 0.011	0.219/ 0.227	0.409/ 0.424
		±0.05°	0.074/ 0.077	0.115/ 0.112	2.160/ 2.261	4.042/ 4.223
	φ	±0.0005°	0.001/ 0.001	0.001/ 0.001	0.001/ 0.001	0.009/ 0.009
		±0.005°	0.012/ 0.011	0.007/ 0.006	0.012/ 0.013	0.087/ 0.088
		±0.05°	0.109/ 0.112	0.056/ 0.062	0.134/ 0.131	0.789/ 0.867
	κ	±0.0008°	0.001/ 0.001	0.002/ 0.002	0.018/ 0.019	0.031/ 0.032
		±0.008°	0.009/ 0.010	0.014/ 0.015	0.174/ 0.190	0.298/ 0.324
		±0.08°	0.099/ 0.100	0.144/ 0.154	1.770/ 1.898	3.021/ 3.243
Refractive index	n_w	±0.007	0.000/ 0.000	0.000/ 0.000	0.003/ 0.003	0.009/ 0.009
		±0.010	0.000/ 0.000	0.000/ 0.000	0.003/ 0.004	0.011/ 0.011
		±0.013	0.000/ 0.000	0.000/ 0.000	0.005/ 0.005	0.015/ 0.017
I.O.	(x_0, y_0)	±0.003mm	0.014/ 0.013	0.012/ 0.013	0.000/ 0.000	0.000/ 0.000
		±0.007mm	0.028/ 0.029	0.029/ 0.029	0.000/ 0.000	0.001/ 0.001
		±0.01mm	0.042/ 0.042	0.039/ 0.042	0.000/ 0.000	0.001/ 0.001
	f	±0.5mm	0.000/ 0.000	0.000/ 0.000	2.067/ 2.104	2.014/ 2.050
		±0.8mm	0.000/ 0.000	0.000/ 0.000	3.115/ 3.393	3.036/ 3.307
		±1.0mm	0.000/ 0.000	0.000/ 0.000	3.922/ 4.254	3.819/ 4.137

From the results presented Table 4, it could be concluded in the assumption of simulated scene that most of the positioning precision get degraded as the error of parameters become larger. However, there are some parameters which are nothing to do with the results of modulation. For example, the refractive index of water medium (n_w), principal distance (f) or (Z_L) in E.O.P., where the quality of factors has no influence on horizontal positioning precision; also, the error of image coordinates of principal point (x_0, y_0) have very little impact on both the vertical positioning precision and the water surface.

4.4 Accuracy Analysis on Water Surface (σ_d) in Stereo-Pair Intersection Using Multiple Points

Considering in the practical application, the point distribution often need to be filled with the overall experimental scene, so the selection, such as 3x3, 4x4 or 6x6 evenly distributed in the measured plane, is chosen in the following experiments. For multiple points intersection, the calculated quality of water surface and underwater object point coordinates corresponding to different number of points (pts) are drawn as below in Figure 11.

(a) (b) (c)

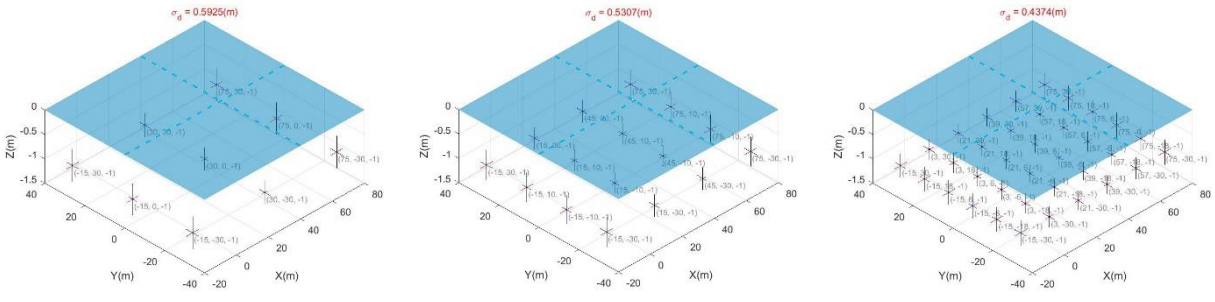

3*3 = 9pts 4*4 = 16pts 6*6 = 36pts

Figure 11. The quality of water surface and each point corresponding to different number of multiple points.

According to the selection of multiple points in Figure 11(c), by means of adding one by one to join the multi-point solution, to observe that how many chosen points at the same time can effectively enhance the stability of the results.

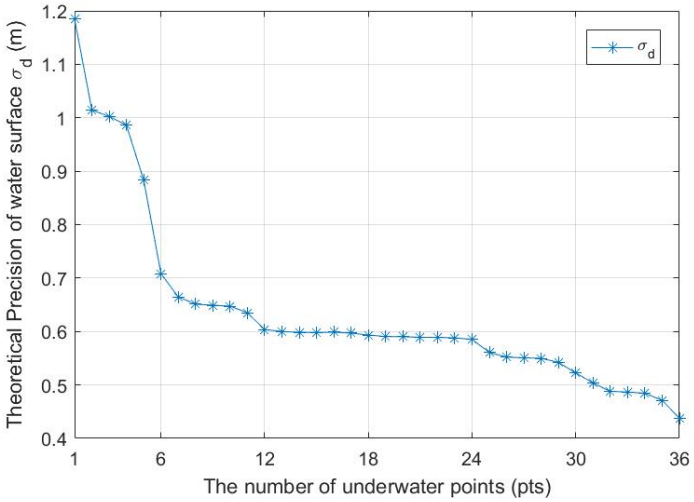

Figure 12. The theoretical precision of water surface (σ_d) in multiple points intersection (1~36pts).

From the results of the positioning accuracy of the water surface in Figure 12, it can be found that when more than 36 added points are solved simultaneously, the results meet our expectations and the optimal positioning accuracy of water surface is about 0.4375 meters. Compared with the single point of the previous results, the positioning accuracy of water surface changes about 800mm. It can be seen that the trend of the outcome appears that adding more points into the intersection is really helpful for the determination of the water surface. However, it is not easy to obtain the point where the above conditions are obtained. Therefore, it is necessary to analyze the different combinations of multiple points to obtain the best positioning quality.

4.5 Results of Single Point/Two Points by Stereo-Pair Intersection

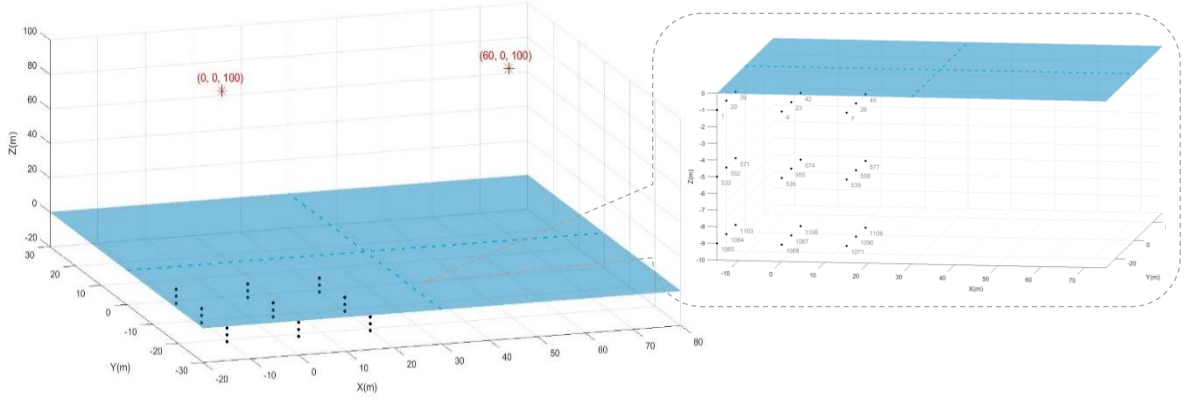

Figure 13. The target points and simulated configuration.

In order to study on air-to-water intersection solving for water surface and three-dimensional coordinates of underwater object points, in the simulation scene, the use of a single quadrant of different locations or depth of the underwater objects to observe the positioning accuracy of the intersection (Figure 13). The results are shown in Table 5, where the theoretical precision is consistent with the empirical accuracy, so that it can be used to judge the correctness of geometric illustrations discussed in the former section.

Table 5. Results from single point photogrammetry intersection.

Point num.	Object Coordinates(m)			Quality of object point coordinates (m)			Quality of water surface (m)	Incident angle (˚)	
	X_A	Y_A	Z_A	±RMSE$_X$/ $\pm\tilde{\sigma}_X$	±RMSE$_Y$/ $\pm\tilde{\sigma}_Y$	±RMSE$_Z$/ $\pm\tilde{\sigma}_Z$	±RMSE$_d$/ $\pm\tilde{\sigma}_d$	α_L	α_R
1	-15	-30	-1	0.039/ 0.042	0.032/ 0.039	0.535/ 0.648	0.994/ 1.185	18.40˚	38.74˚
533	-15	-30	-5	0.041/ 0.043	0.039/ 0.040	0.655/ 0.705	1.222/ 1.314	17.93˚	38.00˚
1065	-15	-30	-9	0.049/ 0.044	0.050/ 0.041	0.849/ 0.766	1.569/ 1.453	17.47˚	37.30˚
23	0	-20	-1	0.025/ 0.027	0.027/ 0.030	0.980/ 1.149	2.197/ 2.610	11.24˚	32.14˚

555	0	-20	-5	0.032/ 0.028	0.026/ 0.031	1.102/ 1.268	2.541/ 2.918	10.90°	31.43°
1087	0	-20	-9	0.026/ 0.028	0.027/ 0.031	1.293/ 1.388	3.014/ 3.234	10.62°	30.76°
45	15	-10	-1	0.049/ 0.048	0.021/ 0.022	4.140/ 3.886	10.986/ 10.322	10.15°	24.60°
577	15	-10	-5	0.039/ 0.049	0.022/ 0.023	3.410/ 4.327	9.092/ 11.569	9.85°	23.98°
1109	15	-10	-9	0.042/ 0.051	0.025/ 0.023	4.094/ 4.795	11.018/ 12.902	9.58°	23.41°

As mentioned above, the results from simultaneously determination of both one water surface and one object point as unknown parameters are different everywhere. The point approaching the center of scene will lead to poorer quality for Z-component and water surface. Also, the deeper the depth, the greater the error in coordinates and water surface. This has to be contributed to the aspects that the horizontal component error will be smaller depending on the decrease of incident angle at the same horizontal position; however, at the same vertical position, the deeper the depth of the water, the smaller corresponding incident angle, but will make the greater the impact of the refraction.

Table 6. Results from two points photogrammetry intersection.

Image	**Point num.**	**Object Coordinates(m)**			**Quality of object point coordinates (m)**			**Quality of water surface (m)**
		X_A	Y_A	Z_A	$\pm$**RMSE**$_X$/ $\pm\tilde{\sigma}_X$	$\pm$**RMSE**$_Y$/ $\pm\tilde{\sigma}_Y$	$\pm$**RMSE**$_Z$/ $\pm\tilde{\sigma}_Z$	$\pm$**RMSE**$_d$/ $\pm\tilde{\sigma}_d$
2(1, 3)	**1**	-15	-30	-1	0.034/ 0.041	0.029/ 0.038	0.458/ 0.591	0.852/ 1.078
	23	75	-30	-1	0.029/ 0.027	0.022/ 0.024	0.382/ 0.482	($\hat{\sigma}_0 = 1.365$)
2(1, 3)	**1**	-15	-30	-1	0.039/ 0.042	0.037/ 0.039	0.619/ 0.644	1.158/ 1.176
	45	15	-10	-1	0.022/ 0.022	0.020/ 0.020	0.453/ 0.451	($\hat{\sigma}_0 = 0.950$)
2(1, 3)	**1**	-15	-30	-1	0.036/ 0.039	0.030/ 0.035	0.413/ 0.486	0.759/ 0.879
	533	-15	-30	-5	0.037/ 0.039	0.033/ 0.034	0.418/ 0.478	($\hat{\sigma}_0 = 1.130$)
2(1, 3)	**45**	15	-10	-1	0.039/ 0.038	0.023/ 0.021	2.864/ 2.907	7.612/ 7.718
	577	15	-10	-5	0.037/ 0.037	0.021/ 0.022	2.862/ 2.887	($\hat{\sigma}_0 = 0.748$)

5. DISCUSSION AND CONCLUSION

From the above results and simulation, it can be concluded that in air-to-water photogrammetry, if only considering one object point for positioning while determining water surface, the solution system renders itself as weak geometry with not only high condition number but also high correlation between Z of the object point and water surface (d), thus resulting in relatively worse quality for these two components. On the other hand, the condition number would dramatically decrease if adding more points into intersection and thus improve the parameter estimations both for water surface and underwater object points. However, the effective strategy in combining few points still awaits further exploitation, as partly illustrated in Table 6.

6. FUTURE WORK

To further enhance the solution quality, the addition of priori information of water surface, if available, would directly benefit the overall solution. On the other hand, priori information for some object points would serve as control information to strengthen the solution network. Moreover, multi-ray intersection is alternative to better the air-to-water photogrammetric intersection.

7. REFERENCE

Chiu, T.H., Jaw, J.J., 2016. Photogrammetric Determination of Water Surface and Underwater Object Points. The 35th Symposium on Surveying and Geospatial Information, Taipei, Taiwan (in Chinese).

Huang, S.J., Jaw, J.J., 2014. Air-to-water Photogrammetric Intersection. The 33th Symposium on Surveying and Geospatial Information, Taipei, Taiwan (in Chinese).

Kotowski, R., 1987. Zur Berücksichtigung lichtbrechender Flächen im Strahlenbündel. Schriftreihe der DGK, Reihe C, Vol. 330.

Maas, H.G., Gruen, A., 1995. Digital photogrammetric techniques for high-resolution 3-D flow velocity measurements. Opt. Eng., 34(7), pp. 1970-1976.

Maas, H.G., 2015. On the Accuracy Potential in Underwater/Multimedia Photogrammetry. Sensors, 15, pp. 18140-18152.

Mikhail, E.W., 1976. Observations and Least Squares. IEP Don-Donnelley, New York, Hagerstown, San Francisco, London.